KEKB Accelerator

Accelerator design at SuperKEKB

Yukiyoshi Ohnishi*, Tetsuo Abe, Toshikazu Adachi, Kazunori Akai, Yasushi Arimoto,
Kiyokazu Ebihara, Kazumi Egawa, John Flanagan, Hitoshi Fukuma, Yoshihiro Funakoshi,
Kazuro Furukawa, Takaaki Furuya, Naoko Iida, Hiromi Iinuma, Hoitomi Ikeda,
Takuya Ishibashi, Masako Iwasaki, Tatsuya Kageyama, Susumu Kamada,
Takuya Kamitani, Ken-ichi Kanazawa, Mitsuo Kikuchi, Haruyo Koiso, Mika Masuzawa,
Toshihiro Mimashi, Takako Miura, Takashi Mori, Akio Morita, Tatsuro Nakamura,
Kota Nakanishi, Hiroyuki Nakayama, Michiru Nishiwaki, Yujiro Ogawa, Kazuhito Ohmi,
Norihito Ohuchi, Katsunobu Oide, Toshiyuki Oki, Masaaki Ono, Masanori Satoh,
Kyo Shibata, Masaaki Suetake, Yusuke Suetsugu, Ryuhei Sugahara, Hiroshi Sugimoto,
Tsuyoshi Suwada, Masafumi Tawada, Makoto Tobiyama, Noboru Tokuda,
Kiyosumi Tsuchiya, Hiroshi Yamaoka, Yoshiharu Yano, Mitsuhiro Yoshida,
Shin-ichi Yoshimoto, Demin Zhou, and Zhanguo Zong

High Energy Accelerator Research Organization, KEK, Oho 1-1, Tsukuba, Ibaraki 305-0801, Japan
*E-mail: yukiyoshi.onishi@kek.jp

. . . .
The SuperKEKB project requires a positron and electron collider with a peak luminosity of 8×10^{35} cm^{-2} s^{-1}. This luminosity is 40 times that of the KEKB B-factory, which operated for 11 years up to 2010. SuperKEKB is an asymmetry-energy and double-ring collider; the beam energy of the positron (LER) is 4 GeV and that of the electron (HER) is 7 GeV. An extremely small beta function at the interaction point (IP) and a low emittance are necessary. In addition, in order to achieve the target luminosity, a large horizontal crossing angle between two colliding beams is adopted, as is a bunch length much longer than the beta function at the IP. This method is called the "nano-beam scheme". The beam–beam parameter is assumed to be similar to KEKB, the beta function at the IP is 1/20, and the beam currents are twice those of KEKB in the nano-beam scheme. Consequently, the luminosity gain of 40 with respect to KEKB can be obtained.
. . . .

1. Introduction

The target luminosity of SuperKEKB is 8×10^{35} cm^{-2} s^{-1}, a goal that comes from physics requirements. The SuperKEKB collider will be constructed by reusing most of the components of KEKB [1,2]. However, there are also many components that need to be modified or newly developed. In order to achieve the target luminosity of 8×10^{35} cm^{-2} s^{-1}, which is 40 times as high as the peak luminosity of KEKB, the vertical beta function at the interaction point (IP) needs to be squeezed down to 1/20 and the beam current needs to be increased to twice that of KEKB while keeping the same beam–beam parameter in the vertical direction as KEKB.

It has been confirmed both theoretically and experimentally at KEKB that a beam–beam parameter up to ~0.09 can be achieved in a collision. However, prediction of the beam–beam limit is very difficult because the phenomenon has nonlinear dynamics, six-dimensional motion, and interactions between many particles. Further improvement of the beam–beam limit is not expected in the design of SuperKEKB.

The vertical beta function at the IP will be squeezed to 270–300 µm while the bunch length is 5–6 mm long. In order to avoid luminosity degradation due to an hourglass effect, the "nano-beam scheme" proposed by P. Raimondi is adopted [3]. Final-focusing quadrupole magnets are to be located nearer to the IP than those of KEKB. The crossing angle is 83 mrad, to satisfy the requirements of the nano-beam scheme and to keep the beams separated in the quadrupole magnets. Simultaneously, not only will the horizontal beta function be squeezed to 25–32 mm but also the horizontal emittance will be reduced to 3.2–4.6 nm to realize nano-beam collision. A vertical emittance is also one of the keys to obtaining higher luminosity in the nano-beam scheme. The ratio of vertical to horizontal emittance is required to be less than ∼0.27% under the influence of the beam–beam interaction, which is a very small coupling compared with circular colliders for elementary-particle physics.

The beam current of the low-energy ring (LER) needs to be increased to 3.6 A and that of the high-energy ring (HER) to 2.6 A to achieve the target luminosity. Improvement and reinforcement of the RF system is required to achieve the design beam currents. The vacuum system is also upgraded to store the high beam currents. Antechambers with a TiN coating [4] are adopted in the LER to reduce electron cloud instabilities. The beam energy of the positron (LER) is 4 GeV and that of the electron (HER) is 7 GeV. Improvements to the injector linac and a damping ring for the positron beam will be necessary because of the shorter beam lifetime and the small dynamic aperture of the rings. The extremely low beta function at the IP makes the dynamic aperture small in general. The design of the interaction region is very restricted by aperture issues. Five big issues (FBI) are addressed in this article:

(1) Touschek lifetime determined by dynamic aperture,
(2) machine error and optics correction,
(3) injection under the influence of beam–beam interaction,
(4) detector background and collimator,
(5) beam energy.

The KEKB collider achieved a luminosity of $2.1 \times 10^{34} \, \text{cm}^{-2} \, \text{s}^{-1}$ in 2009. The design of SuperKEKB is based on the new concept of the nano-beam scheme, including an evolution of the experience of KEKB. A luminosity of $8 \times 10^{35} \, \text{cm}^{-2} \, \text{s}^{-1}$ is a new frontier for the next generation of B factories.

2.   Machine parameters

2.1.   Luminosity

The luminosity is the interaction rate per unit cross section for colliding particles. The number of physics events observed is written as

$$N = \int_0^T L\sigma \, dt, \tag{1}$$

where L is the luminosity, σ is the cross section that is determined by a natural law, and T is the duration of the experiment, typically about 10 years. In order to make the statistical error small enough, namely, to increase the number of physics events, it is necessary to increase the luminosity. The luminosity can be expressed as

$$L = \frac{\gamma_\pm}{2er_e} \left(1 + \frac{\sigma_y^*}{\sigma_x^*}\right) \left(\frac{I_\pm \xi_{y\pm}}{\beta_y^*}\right) \left(\frac{R_L}{R_{\xi_{y\pm}}}\right), \tag{2}$$

where "+" denotes positrons and "−" denotes electrons for the positron–electron collider. In the above expression, $\sigma_{x,y}^*$ is the beam size at the IP in the horizontal and vertical plane, I the beam current, β_y^* the vertical beta function at the IP, $\xi_{y\pm}$ the vertical beam–beam parameter, R_L and $R_{\xi_{y\pm}}$ the reduction factors for the luminosity and the beam–beam parameter, r_e the classical electron radius, and γ the Lorentz factor. It is assumed that the vertical beta function and the transverse beam size of the positron beam are the same as the electron beam. The parameters of the horizontal beta function at the IP, the horizontal emittance, the bunch length, and the crossing angle between two beams that are not included in Eq. (2) contribute the luminosity through the beam–beam parameter and the reduction factors due to geometrical loss such as the hourglass effect and finite crossing. Therefore, the formula tells us that the luminosity is proportional to the beam–beam parameter and the beam current, and inverse of the vertical beta function at the IP.

The vertical beam–beam parameter is described by

$$\xi_{y\pm} = \frac{r_e}{2\pi\gamma_\pm} \frac{N_\mp \beta_y^*}{\sigma_y^*(\sigma_x^* + \sigma_y^*)} R_{\xi_{y\pm}} \propto \frac{N_\mp}{\sigma_x^*} \sqrt{\frac{\beta_y^*}{\varepsilon_y}}, \tag{3}$$

where N is the number of particles in a bunch. The beam–beam parameter is limited by the nonlinear force in a circular collider and a maximum value of about 0.02–0.1 has been obtained from various colliders in 40 years. The beam–beam parameter increases on increasing the bunch population. However, the vertical emittance becomes large when the beam–beam parameter reaches the beam–beam limit. Then, the luminosity is only proportional to one of the beam currents and becomes a constant value as a result of compensating the increase of the beam current for a decrease of the beam–beam parameter. If we can maintain the ratio of the vertical beta function to the vertical emittance with a constant beam current, the vertical beta function can be squeezed with a constant beam–beam parameter.

In case of a head-on collision, the beta function at the IP cannot be squeezed smaller than the bunch length, since the hourglass effect decreases the luminosity. The bunch length should be small in order to achieve the small beta function at the IP; however, there are some difficulties in making the bunch length small. One serious problem is coherent synchrotron radiation (CSR). Another difficulty is HOM loss or HOM heating, which might damage vacuum components such as bellows.

2.2. Beam energy

The beam energy is determined by the purpose of the physics of interest. The center of mass energy of $\Upsilon(4S)$ is a main target in SuperKEKB. The asymmetric beam energy is required to identify and to measure the vertexes of particle decays. The beam energies in SuperKEKB are 4 GeV in the LER and 7 GeV in the HER, instead of 3.5 GeV and 8 GeV in KEKB. The boost factor has also been changed; however, the impact on physics is restrictive and small. Consequently, the emittance growth due to intra-beam scattering can be reduced and the Touschek lifetime can be improved in the LER compared to 3.5 GeV. The emittance in the HER can also be reduced and the design value is achieved by changing the beam energy together with the lattice design.

Figure 1 shows the flexibility of the beam energy of the LER and the HER, respectively. The range of beam energy covers the $\Upsilon(1S)$ and $\Upsilon(6S)$ resonance states for the physics operation. The maximum center of energy is 11.24 GeV in SuperKEKB due to the maximum beam energy of the injector linac. On the other hand, with a beam energy much lower than $\Upsilon(1S)$, for instance around of τ threshold, the lattice design becomes difficult unless the detector solenoid field is scaled proportional to the beam energy.
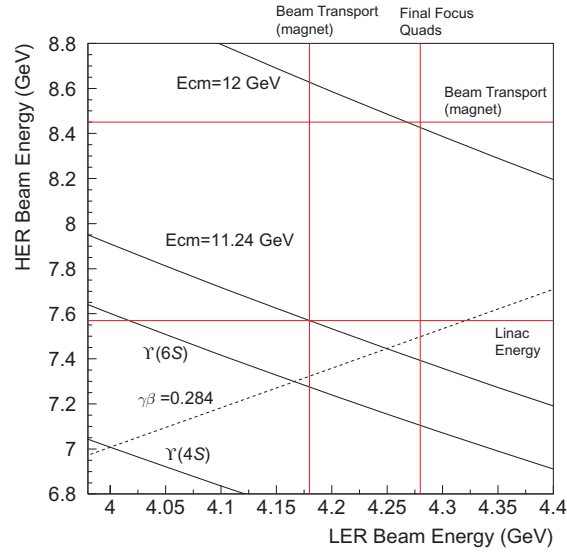
Fig. 1. Beam energies to achieve the center of mass energies, $\Upsilon(4S)$, $\Upsilon(6S)$, 11.24 GeV, and 12 GeV. The horizontal axis is the LER beam energy and the vertical axis the HER beam energy.

2.3. Nano-beam scheme

One of the keys for a high luminosity collider is how to make an extremely low beta function at the IP. In order to overcome the hourglass effect for a relatively long bunch length, a small beam size at the IP with a large Piwinski angle is applied. The overlap area with the small spot size at the IP is localized and the length of the overlap area can be written as

$$d = \frac{\sigma_x^*}{\sin \phi_x}, \tag{4}$$

where ϕ_x is the half-crossing angle. The overlap length, d, is the effective bunch length, which is much shorter than the bunch length along the beam axis and should be compared to the vertical beta function for the hourglass effect. The vertical beta function should satisfy this hourglass requirement:

$$\beta_y^* \geq d = \frac{\sigma_x^*}{\sin \phi_x}. \tag{5}$$

In order to squeeze the vertical beta function at the IP, the effective bunch length, d, is decreased by decreasing the horizontal spot size at the IP and increasing the crossing angle.

On the other hand, the spot size in the horizontal direction effectively becomes $\sigma_z \sin \phi_x$, which is larger than the nominal σ_x^*. The luminosity formula (Eq. (2)) and the beam–beam parameter (Eq. (3)) are modified by replacing σ_x^* with the effective spot size, $\sigma_z \sin \phi_x$. The horizontal beam–beam parameter in the nano-beam scheme can be small compared with the general head-on scheme:

$$\xi_{x\pm} = \frac{r_e}{2\pi \gamma_\pm} \frac{N_\mp \beta_x^*}{\sigma_x^*(\sigma_x^* + \sigma_y^*)} R_{\xi_{x\pm}} \propto \frac{N_\mp \beta_x^*}{(\sigma_z \sin \phi_x)^2}, \tag{6}$$

where we assume that the beta function and the bunch length, σ_z, are the same for the positrons and the electrons. The dynamic effect due to beam–beam interactions such as a dynamic beta function and a dynamic emittance in the horizontal direction, which causes an aperture problem, can be reduced in the nano-beam scheme since the horizontal beam–beam parameter is small. The betatron tune in the horizontal direction is chosen to be above $2\nu_x + \nu_s =$ integer to avoid a strong synchro-beta

Table 1. Machine parameters. * indicates values at the IP.

	LER	HER	Unit
E	4.000	7.007	GeV
I	3.6	2.6	A
N_b	2500		
C	3016.315		m
ε_x	3.2	4.6	nm
ε_y	8.64	11.5	pm
β_x^*	32	25	mm
β_y^*	270	300	μm
$2\phi_x$	83		mrad
α_p	3.25×10^{-4}	4.55×10^{-4}	
σ_δ	8.08×10^{-4}	6.37×10^{-4}	
V_c	9.4	15.0	MV
σ_z	6	5	mm
ν_s	-0.0247	-0.0280	
ν_x	44.53	45.53	
ν_y	44.57	43.57	
U_0	1.87	2.43	MeV
τ_x/τ_s	43.1/21.6	58.0/29.0	msec
ξ_x	0.0028	0.0012	
ξ_y	0.0881	0.0807	
L	8×10^{35}		$\mathrm{cm}^{-2}\,\mathrm{s}^{-1}$

resonance. This is different from the KEKB operation; in particular, the horizontal tune is chosen to be below $2\nu_x + \nu_s =$ integer in the KEKB-LER.

Table 1 shows the machine parameters of SuperKEKB. The effect of intra-beam scattering is included. The vertical emittance is estimated from the sum of contributions from the beam–beam interaction and an orbit distortion due to a solenoid field in the vicinity of the IP and so on. When a crossing angle of 83 mrad, an emittance of 3.2 nm, and a horizontal beta function of 32 mm are chosen, the vertical beta function can be squeezed up to 244 μm while the bunch length is 6 mm in the LER. The vertical beam–beam parameter is assumed to be 0.09 at the maximum shown in Table 1. The beam–beam limit in the design parameters is determined by our experience of the KEKB operation. Finally, the beam currents are determined in order to achieve the target peak luminosity of 8×10^{35} $\mathrm{cm}^{-2}\,\mathrm{s}^{-1}$. The beam currents for SuperKEKB become approximately twice those of KEKB.

3. Lattice design

3.1. Low emittance

The equilibrium emittance is determined by the ratio of diffusion due to quantum excitation to radiation damping. The emittance can be expressed by radiation integral formulae in the case without either X–Y coupling or Z–X coupling:

$$\varepsilon_x = \frac{C_\gamma \gamma^2}{J_x} \frac{I_5}{I_2}, \quad I_2 = \oint \frac{ds}{\rho^2}, \quad I_5 = \oint \frac{H}{|\rho^3|} ds, \tag{7}$$

where

$$C_\gamma = \frac{55}{32\sqrt{3}} \frac{\hbar c}{m_e c^2}, \quad H = \gamma_x \eta_x^2 + 2\alpha_x \eta_x \eta_{p_x} + \beta_x \eta_{p_x}^2, \tag{8}$$

J_x is the damping partition number, ρ the curvature of dipole magnets, $\alpha_x, \beta_x, \gamma_x$ horizontal Twiss parameters, and η_x, η_{p_x} horizontal dispersion functions in the normal coordinate. In order to make the emittance small, it is necessary to reduce the integration of H in the dipole magnets, to make the
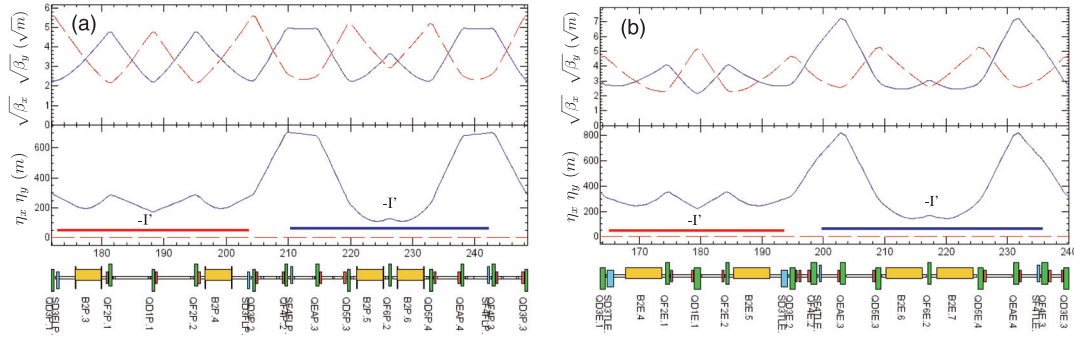
Fig. 2. Non-interleaved 2.5 π arc lattice. (a) LER, (b) HER.

curvature of the dipole magnets large, and to make the damping partition number large at the fixed beam energy.

The requirements are that the quadrupole magnets of KEKB are reused as much as possible and the magnet configuration for the arc section in SuperKEKB is almost the same as in KEKB. The dipole magnets are replaced by a length of 4.2 m instead of 0.89 m to obtain the low emittance in the LER. On the other hand, the beta functions and dispersions are modified to make the emittance as small as possible in the HER because the dipole magnet length in KEKB is already sufficient. The lattice design of the arc cell is shown in Fig. 2.

Wiggler magnets are also installed in each ring to make the emittance small in addition to the modification of the arc lattice. The emittance is modified by

$$\varepsilon_x = \frac{C_\gamma \gamma^2}{J_x} \frac{I_{5,\text{arc}} + I_{5,\text{wiggler}}}{I_{2,\text{arc}} + I_{2,\text{wiggler}}}, \tag{9}$$

where the suffixes arc and wiggler indicate the region of the integration. In the case of the LER, the emittance becomes 1.87 nm with the wiggler section although the emittance of the arc cell is 4.08 nm.

Another way to decrease the emittance is by the frequency-shift method [5,6]. The damping partition number is expressed by

$$J_x = 1 - \frac{I_4}{I_2}, \quad I_4 = \oint \frac{1}{\rho^2} \left(\frac{1}{\rho} + 2\rho K_1 \right) \eta_x ds, \tag{10}$$

where K_1 is the field gradient of the quadrupole magnets. In the case of a non-combined quadrupole magnet, ρK_1 is zero. However, when an orbit offset in the quadrupole magnet, Δx, is applied, the change in I_4 can be shown by replacing $1/\rho$ with $K_1 \Delta x$:

$$\Delta I_4 \simeq \oint 2K_1^2 \eta_x \Delta x ds, \tag{11}$$

where the orbit offset can be induced by a frequency shift in the RF system. Consequently, the change of the damping partition number can be written as

$$\Delta J_x = -\frac{1}{I_2} \oint 2K_1^2 \eta_x^2 \frac{\Delta p}{p_0} ds, \quad \frac{\Delta p}{p_0} = -\frac{1}{\alpha_p} \frac{\Delta f_{\text{RF}}}{f_{\text{RF}}}, \tag{12}$$

where α_p is the momentum compaction factor and f_{RF} is the RF frequency. Thus, the emittance can be decreased by increasing the RF frequency when the momentum compaction factor is positive.
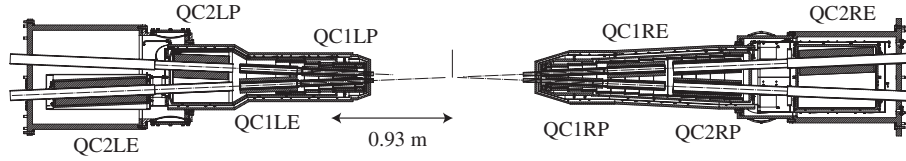
Fig. 3. The layout of the final-focus magnets.

Conversely, the momentum spread is increased by decreasing I_4 to reduce the emittance as follows:

$$(\sigma_\delta)^2 = C_\gamma \gamma^2 \frac{I_3}{2I_2 + I_4}, \quad I_3 = \oint \frac{ds}{|\rho^3|}. \tag{13}$$

The bunch length is also increased according to the momentum spread. In SuperKEKB, the frequency-shift method is not suitable since an increase in the energy spread is unsuitable for B-factory experiments and the dynamic aperture becomes another issue.

3.2. Low beta function at the IP

The final focus (FF) is designed to achieve an extremely low beta function at the IP. In order to squeeze the beta functions, doublets of vertical focus quadrupole magnets (QC1s) and horizontal focus quadrupole magnets (QC2s) are utilized [7]. The QC1 magnets are nearer the IP than the QC2 magnets, which are independent magnets for each ring. The magnet system consists of superconducting magnets. These magnets have correction coils of a dipole, a skew dipole, a skew quadrupole, and an octupole field. Iron shields to suppress the leakage field to the opposite beam are attached to the QC1s and QC2s except for the QC1s (QC1LP and QC1RP) in the LER. Since there is no space for the iron shield for the QC1s in the LER, the leakage field to the HER beam has to be considered. Cancel coils are adopted in the HER to compensate the sextupole, octupole, decapole, and dodecapole fields, while the dipole and quadrupole fields are used to adjust the optical functions. Figure 3 shows the layout of the final-focus magnets.

The leakage dipole fields from QC1LP and QC1RP affect the orbit in the HER. The QC1s and QC2s in the HER are shifted parallel to the nominal beam axis by $700\,\mu$m horizontally to make the strength of the dipole fields of the corrector coils in QC1LE and QC1RE in the HER as small as possible. The angle of the dipole corrector in the QC1s is about 1.25 mrad.

A solenoid field of 1.5 T is located in the vicinity of the IP for the Belle II detector. The anti-solenoid magnets overlap with the QC1s and QC2s and are utilized to fully compensate the detector solenoid for each side of the IP as follows:

$$\int_{\text{IP}}^{L} B_z(s) ds = 0, \tag{14}$$

where L is the distance of 4 m from the IP along the beam line in SuperKEKB. Rotation of the final-focus magnets around the beam axis and/or the skew quadrupole corrector is used to make the vertical dispersions and X–Y couplings as small as possible. For instance, the rotation angle of the QC1s and QC2s around the beam axis can be optimized by

$$\theta_{\text{QC}} = \frac{1}{2B\rho} \int_{\text{IP}}^{\text{QC}} B_z(s) ds. \tag{15}$$

Fig. 4. Lattice design of the interaction region. (a) LER, (b) HER.

The fringe field due to the crossing angle between the beam and the solenoid axis induces the vertical emittance. The skew dipole field from the fringe is expressed by

$$B_x(s) \simeq -\frac{x}{2}B_z'(s) = -\frac{s\phi_x}{2}B_z'(s), \tag{16}$$

where ϕ_x is 41.5 mrad, the half-crossing angle in SuperKEKB. We use the skew dipole corrector in the QC1s and QC2s to adjust the vertical orbit to connect the outer region of the solenoid field smoothly to the plane. In order to reduce the vertical emittance, the derivative of B_z should be reduced as much as possible. The vertical emittance from the solenoid fringe becomes 1.5 pm for the LER and the HER, respectively. The residual X–Y coupling and vertical dispersion are corrected by using skew quadrupole magnets and/or skew dipole magnets, which are located between the FF and a local chromaticity correction region. The lattice design of the IR is shown in Fig. 4.

3.3.　Local chromaticity correction

The natural chromaticity is $\xi_{x0} = -104$ and $\xi_{y0} = -738$ in the LER and $\xi_{x0} = -161$ and $\xi_{y0} = -1073$ in the HER, respectively. Since approximately 80% of the natural chromaticity in the vertical direction is induced in the FF, a local chromaticity correction (LCC) is adopted to correct the large chromaticity near the FF. The LCC consists of two identical sextupole magnets. The transfer matrix between two sextupoles is $-I'$ to compensate the nonlinear kick due to the strong field of the sextupoles,

$$\begin{pmatrix} -1 & 0 & 0 & 0 \\ m_{21} & -1 & 0 & 0 \\ 0 & 0 & -1 & 0 \\ 0 & 0 & m_{43} & -1 \end{pmatrix}. \tag{17}$$

There are two families of sextupole magnets; one is for the vertical chromaticity correction (Y-LCC) and the other is for the horizontal one (X-LCC). The phase advance between QC1 and the Y-LCC is π in the vertical direction and that between QC2 and the X-LCC is 2π in the horizontal direction for each side of the IP. Horizontal dispersions are made at the LCC by using several dipole magnets. Figure 5 shows the lattice design of the LCC region.

Fig. 5. Lattice design of the local chromaticity corrections. (a) LER, (b) HER.

3.4. *Dynamic aperture*

It is difficult to apply either an analytic approach or a perturbative method to an evaluation of the dynamic aperture, since, for instance, the sextupole magnets cause strong nonlinear effects. Therefore, the dynamic aperture is estimated by numerical tracking simulations. A particle-tracking simulation has been performed by using SAD [8], an integrated code for optics design, particle tracking, matching tuning, and so on, that has been successfully used for years at several accelerators such as KEKB and KEK-ATF. Six canonical variables, x, p_x, y, p_y, z, and δ are used to describe the motion of a particle, where p_x and p_y are transverse canonical momenta normalized by the design momentum, p_0, and δ is the relative momentum deviation from p_0. Synchrotron oscillation is included while synchrotron radiation and quantum excitation are turned off during tracking simulations.

The FF region within ± 4 m from the IP, the magnetic field of Belle II, the compensation solenoids, and the QCs (QC1 and QC2) along the longitudinal direction on the beam line are sliced by a thickness of 10 mm of constant B_z or $K_1 = B'L/B\rho$ to make the lattice model. Higher-order multipole fields of up to 44 poles for normal and skew fields are included in the slices [9]. The three-dimensional solenoid field is calculated by using ANSYS [10], which is an electromagnetic field simulation code. The behavior of the solenoid field is also implemented by slices in the model [11]. The fringe field of the solenoid field and higher-order multipole fields of the final-focus magnets significantly affect the dynamic aperture.

The arcs of the SuperKEKB rings consist of 2.5π unit cells that include non-interleaved sextupole pairs for chromaticity corrections. Two non-interleaved sextupole magnets are placed in a cell, and the number of sextupole pairs in the whole ring amounts to 50. Two sextupole magnets in a pair are connected with a $-I'$ transformer. By this arrangement, the principle nonlinearities of the sextupoles are canceled in each pair, which creates a large transverse dynamic aperture.

The larger dynamic aperture is obtained by optimizing 54 families of sextupoles and 12 families of skew sextupoles in both the arc and the LCC, and 4 families of octupole coils in the QCs. The optimization utilizes off-momentum matching and the downhill simplex method as a function of the area of the dynamic aperture. The dynamic aperture is important for maintaining sufficient Touschek lifetime as well as the injection aperture. Figure 6 shows the dynamic aperture in the LER and the HER, respectively. The area of the dynamic aperture is fitted by an ellipse to estimate the Touschek lifetime. Two initial betatron phases of $(0, 0)$ and $(\pi/2, \pi/2)$ in the horizontal and vertical planes are calculated in the dynamic aperture survey. The Touschek lifetime is defined by the average of two cases, since the larger betatron amplitude becomes a nonlinear region and the Poincaré plot differs
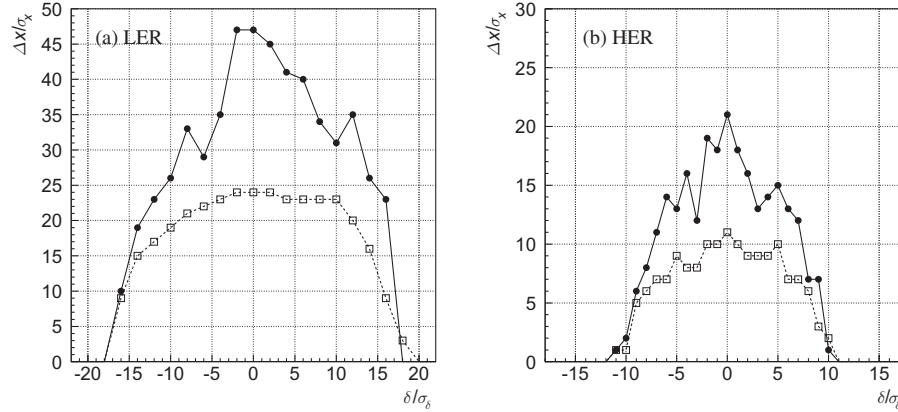
Fig. 6. Dynamic aperture. (a) LER, (b) HER. The closed circles indicate the initial phase of $(0, 0)$; $(\pi/2, \pi/2)$ is represented by the open squares. Synchrotron oscillation is included without synchrotron radiation. The number of turns used to evaluate the stability of the motion is 1000.

from a circle. The Touschek lifetimes of 492 sec in the LER and 603 sec in the HER are obtained from the dynamic aperture. The target for the Touschek lifetime is 600 sec; the requirement is almost satisfied in the ideal lattice and optimization is still continuing.

3.5. *Machine error and optics correction*

The nano-beam scheme requires the ratio of vertical emittance to horizontal emittance to be small. The design value of the emittance ratio is 0.27% in the LER and 0.28% in the HER, respectively, which include the fringe field of the solenoid magnet, the beam–beam interaction, intra-beam scattering, and machine error. Therefore, the machine error contribution should be reduced as much as possible; a tentative target for it is within 0.15% of the emittance ratio for a corrected lattice.

In an X–Y decoupled coordinate system, the canonical variables of a particle can be described as

$$
\begin{pmatrix} X \\ p_X \\ Y \\ p_Y \end{pmatrix} = \begin{pmatrix} \mu & 0 & -r_4 & r_2 \\ 0 & \mu & r_3 & -r_1 \\ r_1 & r_2 & \mu & 0 \\ r_3 & r_4 & 0 & \mu \end{pmatrix} \left\{ \begin{pmatrix} x \\ p_x \\ y \\ p_y \end{pmatrix} - \begin{pmatrix} \eta_x \\ \eta_{p_x} \\ \eta_y \\ \eta_{p_y} \end{pmatrix} \delta \right\}
\tag{18}
$$

and

$$
\mu^2 + (r_1 r_4 - r_2 r_3) = 1,
\tag{19}
$$

where (x, p_x, y, p_y) are physical variables and $(\eta_x, \eta_{p_x}, \eta_y, \eta_{p_y})$ are physical dispersions in a laboratory coordinate system. We refer to (r_1, r_2, r_3, r_4) as X–Y coupling parameters. The X–Y coupling parameters have been measured by the response of closed orbit distortion (COD). The leakage vertical orbits induced by horizontal steering magnets are observed by averaged-mode BPMs (beam-position monitors) and corrected to the model response by using local bump orbits at the sextupole magnets during KEKB operation [12]. On the other hand, the X–Y coupling can be measured by using single-pass BPMs where the bunch is kicked by a kicker [13–15]. The betatron oscillation of a pilot bunch measured by single-pass BPMs is a feasible approach to obtaining optical functions during beam collisions at high current. The relation between the physical variables and the X–Y
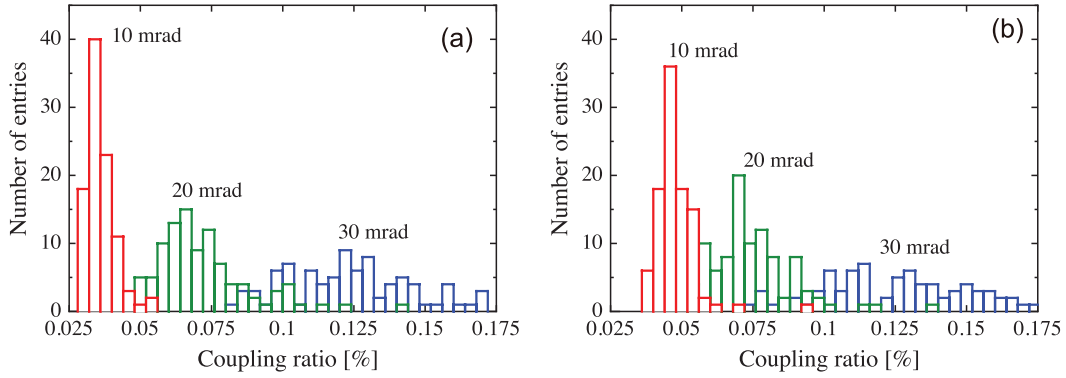
Fig. 7. Emittance ratio after optics corrections with a BPM rotation error. (a) COD-based measurement, (b) measurement of single-pass BPMs.

coupling parameters can be expressed by

$$
\begin{pmatrix} r_1 \\ r_2 \\ r_3 \\ r_4 \end{pmatrix} = -\mu \Sigma^{-1} \begin{pmatrix} \langle xy \rangle \\ \langle xp_x \rangle \\ \langle xp_y \rangle \\ \langle p_x p_y \rangle \end{pmatrix}, \tag{20}
$$

where

$$
\Sigma = \begin{pmatrix} \langle x^2 \rangle & \langle xp_x \rangle + \langle yp_y \rangle & 0 & -\langle y^2 \rangle \\ \langle xp_x \rangle - \langle yp_y \rangle & \langle p_x^2 \rangle & \langle y^2 \rangle & 0 \\ 0 & \langle p_y^2 \rangle & \langle x^2 \rangle & \langle xp_x \rangle - \langle yp_y \rangle \\ \langle p_y^2 \rangle & 0 & \langle xp_x \rangle + \langle yp_y \rangle & \langle p_x^2 \rangle \end{pmatrix}.
$$

Vertical dispersions can be measured by either an RF frequency-shift or an RF kick. Skew quadrupole coils at sextupole magnets correct not only the $X-Y$ coupling parameters but also the vertical dispersions [16]. Figure 7 shows the emittance ratio after optics measurements and corrections. The rotation of quadrupoles around the beam axis, $\sigma_\theta = 100\,\mu\text{rad}$, and the vertical misalignment of sextupoles, $\sigma_{\Delta y} = 100\,\mu\text{m}$, are considered to be a machine error. The resolution of the BPMs is assumed to be $2\,\mu\text{m}$ for the averaged mode (COD measurement) and $100\,\mu\text{m}$ for single-pass BPMs. A BPM rotation error within $10\,\text{mrad}$ around the beam axis is required to correct the vertical emittance to be smaller than the target value.

4.   Injection

SuperKEKB uses "continuous injection" (top-up injection), which is similar to that of KEKB. The injector linac provides an injection beam for four storage rings: the SuperKEKB high-energy electron ring (HER), the low-energy positron ring (LER), the PF-AR (Photon Factory Advanced Ring at KEK) electron ring, and the PF (Photon Factory storage ring at KEK) electron ring. The injection beams for these rings have different energies and intensities. Since continuous injection is necessary to maintain constant luminosity against a short beam lifetime, simultaneous injection among these rings is required at SuperKEKB. Further requirements are a large beam intensity per pulse and a low emittance for both electrons and positrons because the lifetime of the main rings will be $\sim$600 sec at design beam currents and the injection aperture will be small. In order to make this possible, a photo-cathode RF gun is adopted to make electrons and a flux concentrator is used to make positron beams. Two-bunch-per-pulse injection is considered, as well as increasing the beam intensity per

Table 2. Parameters of electron injection. 'H.E.' indicates 'hard edge'.

	ε_x (nm)	ε_y (nm)	σ_z (mm)	σ_δ (%)	E (GeV)
Linac end	1.46	1.46	±3.0 (H.E.)	±0.125 (H.E.)	7.0
Injection point	1.46	1.46	±4.1 (H.E.)	±0.125 (H.E.)	7.0

Table 3. Parameters of positron injection. 'H.E.' indicates 'hard edge'. *99% included.

		ε_x (nm)	ε_y (nm)	σ_z (mm)	σ_δ (%)	E (GeV)
Before DR	Before ECS	1500	1500	±8 (H.E.)	±5 (H.E.)	1.1
	After ECS	1500	1500	±35 (H.E.)	±1.5 (H.E.)	1.1
After DR	Before BCS	42.9	3.12	6.9	0.057	1.1
	After BCS	42.9	3.12	0.76	0.73	1.1
Injection point		11.8	0.86	18.3*	0.24*	4.0

pulse. The RF gun makes a small emittance while the beam intensity is large. Since the positrons coming from the flux concentrator have a large emittance, a damping ring is necessary to make the positron emittance small. The damping ring for positron injection will be newly constructed. The positron beam is accelerated up to 1.1 GeV by the linac and extracted to inject for the damping ring. The circumference of the damping ring is 135 m, to store two bunches. The arc section consists of FODO cells, including reverse dipole magnets, to make the momentum compaction small, which can reduce the damping time. The horizontal damping time is 10.87 msec. The horizontal emittance is reduced from 1.4 μm to 42.9 nm and the vertical emittance from 1.4 μm to 3.12 nm by using the damping ring. The positron beam is injected to the linac again, then accelerated up to 4 GeV and injected to the LER. The emittance at the injection point of the LER is 11.8 nm in the horizontal direction and 0.86 nm in the vertical direction. Table 2 shows the parameters for electron injection; those for positron injection are shown in Table 3.

4.1. Injection under the influence of beam–beam interaction

SuperKEKB uses a multi-turn injection scheme. The multi-turn injection employs a septum magnet with an orbit bump in the vicinity of the septum. The orbit bump induced by the kickers is in the horizontal plane since the horizontal acceptance is larger than the vertical acceptance in a conventional ring. The two kicker units, the betatron phase advance of which is π, move the circulating beam close to the septum during injection. The injected beam is steered to minimize the coherent oscillation. The coherent oscillation is finite due to the thickness of the septum wall. Then, the injected beam performs betatron oscillation around the circulating beam and the betatron oscillation is damped by synchrotron radiation and the bunch-by-bunch feedback system. This is called betatron phase space injection. The transverse damping time is 43 msec for the LER and 58 msec for the HER. The bunch-by-bunch feedback system performs to make the damping of the central orbit for the injected beam fast. The repetition rate of the injection is 25 Hz at maximum during continuous injection, which is similar to the transverse radiation damping rate.

Beam collisions are kept during continuous injection. The nano-beam scheme introduces an extremely low beta function at the collision point with a large Piwinski angle. An injected beam has a finite coherent oscillation in the horizontal direction while it merges into a stored beam, although a local bump orbit between two injection kickers makes the oscillation as small as possible. The horizontal beam position is translated into longitudinal displacement of the collision point due to the large horizontal crossing angle between two colliding beams. This implies that the injected beam collides

with the opposite beam at a large vertical beta function, which comes from the hourglass effect, receiving a large vertical kick. The behavior of the injected beam under the influence of beam–beam interactions should be considered for stable injection to the SuperKEKB rings. In order to overcome the difficulties in the betatron injection, a cure for synchrotron phase space injection [17,18] is considered. The horizontal betatron oscillation can be suppressed in the synchrotron injection. Another cure is a crab waist scheme [3]. In this scheme, the waist position, which is the minimum position of the beta function, is adjusted by a kick from the sextupole magnets to suppress the hourglass effect in the vertical plane. Consequently, the particles collide with the other beam at their waist point, and beam–beam interactions and betatron couplings induced by the large crossing angle are suppressed. However, the crab waist reduces the dynamic aperture significantly due to a nonlinear effect between the IP and sextupole magnets; thus, a breakthrough is necessary.

4.2.   Synchrotron phase space injection

The injection in synchrotron phase space requires non-zero dispersion at the injection point. The local bump orbit is induced by kickers to make the circulating beam close to the septum. The beam is injected with an energy offset. The distance between the injected beam and the circulating beam at the injection point is adjusted by the energy offset of the injected beam:

$$\Delta x = \eta_x \delta_0, \tag{21}$$

where $\delta_0 = \Delta p / p_0$. The energy offset should be within the momentum acceptance and is expressed by

$$\delta_0 < \delta_a - 2\sigma_{\delta, I}, \tag{22}$$

where δ_a is the momentum acceptance of the ring and $\sigma_{\delta, I}$ the energy spread of the injected beam.

On the other hand, the distance requires the condition:

$$\Delta x = n_C \sqrt{\beta_{x,R} \varepsilon_{x,R} + (\eta_x \sigma_{\delta,R})^2} + w_s + n_I \sqrt{\beta_{x,I} \varepsilon_{x,I}}, \tag{23}$$

where $\beta_{x,R}$ and $\beta_{x,I}$ are the beta functions at the injection point and of the injected beam, $\varepsilon_{x,R}$ and $\varepsilon_{x,I}$ are the emittances of the circulating and the injected beams, respectively, $\sigma_{\delta,R}$ is the energy spread of the ring, w_s the thickness of the septum, n_C the number of sigmas of the circulating beam, and n_I the number of sigmas of the injected beam. Figure 8 shows the required dispersion as a function of the beta function at the injection point. The thickness of the septum is 4 mm and the parameters in the HER are used. The momentum acceptance is $10\sigma_{\delta,R}$ in the HER and $\delta_0 = 0.5\%$ is used. The value of n_C is assumed to be 3, and 2.5 for n_I.

5.   Detector background

The performance of SuperKEKB gives 40 times higher luminosity than KEKB with twice the beam currents and 20 times smaller beta functions at the IP. This implies higher beam-induced background in the Belle II detector. The processes causing the detector background in the equilibrium state are:

 (1) Touschek effect
 (2) Beam-gas scattering
     (a) Coulomb scattering
     (b) Bremsstrahlung scattering
 (3) Radiative Bhabha scattering
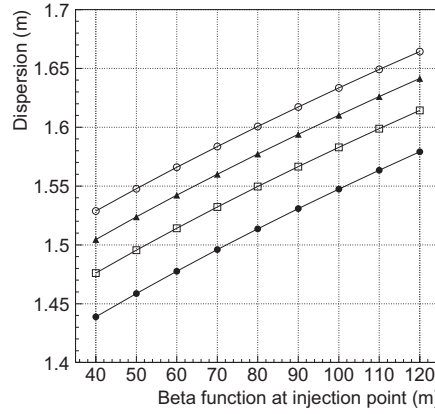 (4) Synchrotron radiation near the IP.

Fig. 8. Requirement of dispersion as a function of beta function at the injection point. The beta function of the injected beam is 10 m for closed circles, 20 m for squares, 30 m for triangles, 40 m for open circles.

We have obtained the result that the detector background is acceptable for Belle II with thick tungsten shields on the cryostat of the final-focus system and neutron shields [19].

The Touschek effect is the transformation of small transverse momentum into large longitudinal momentum due to Coulomb scattering. The Touschek effect is a single scattering effect and the scattered particles are lost if the particles are outside the momentum acceptance. The loss rate is defined by

$$\frac{dN}{dt} = -\frac{N}{\tau} = -R \tag{24}$$

and

$$R = \frac{1}{L_{\text{circ}}} \oint r \, ds, \tag{25}$$

where τ is the lifetime, L_{circ} is the circumference of the ring, and r is the local loss rate. The local loss rate, referred to as Bruck's formula, can be written as

$$r(u_a, \varepsilon_x, \beta_x, \eta_x, \varepsilon_y, \beta_y) = \frac{r_e^2 c \beta_x N^2}{8\pi \gamma^3 \beta \sigma_{x\beta} \sigma_{y\beta} \sigma_z \sigma_x u_a} C(u_a) \tag{26}$$

and

$$C(u_a) = -\frac{3}{2} e^{-u_a} + \int_{u_a}^{\infty} \left(1 + \frac{3}{2} u_a + \frac{u_a}{2} \ln \frac{u}{u_a}\right) e^{-u} \frac{du}{u} \tag{27}$$

$$u_a = \left(\frac{\delta_a \beta_x}{\gamma \sigma_{x\beta}}\right)^2 \tag{28}$$

$$\sigma_x = \sqrt{(\varepsilon_x \beta_x)^2 + \eta_x \sigma_\delta} \tag{29}$$

$$\sigma_{x\beta} = \sqrt{\varepsilon_x \beta_x} \quad \sigma_{y\beta} = \sqrt{\varepsilon_y \beta_y}, \tag{30}$$

where $\sigma_{x\beta}$ and $\sigma_{y\beta}$ are transverse beam-sizes determined by betatron coordinates and δ_a is the momentum acceptance of the ring. This expression is consistent with a non-relativistic and flat-beam approximation of Piwinski's formula. The particle loss with various momentum deviations due to the Touschek effect can be evaluated by particle-tracking simulations along each location in the whole ring. The scattering probability is calculated by Eq. (26). The lower beam energy is sensitive to the Touschek background and the loss rate in the vicinity of the IP for the LER is shown in Fig. 9.
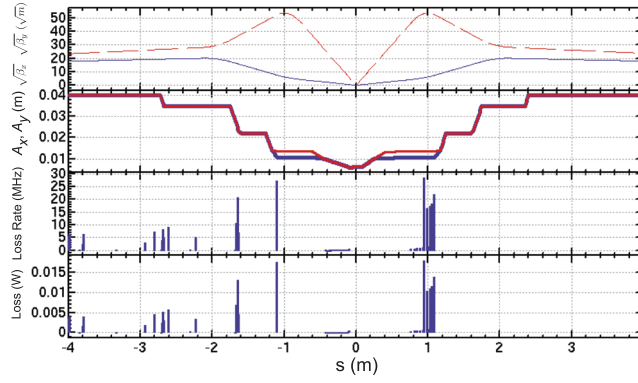
Fig. 9. Loss rate due to the Touschek effect in the vicinity of the IP ($s = 0$) in the LER. The blue line indicates the horizontal direction and red indicates the vertical direction in the upper two rows. The horizontal physical aperture is indicated by A_x, with A_y representing the vertical direction.

The aperture of movable masks located in the upper stream of the IP is required from

$$d_x = \max\left(\sqrt{\frac{\beta_{x,\text{mask}}}{\beta_{x,\text{QC2}}}}\, a_{x,\text{QC2}}, \eta_{x,\text{mask}}\delta_a\right) \tag{31}$$

$$d_y = \max\left(\sqrt{\frac{\beta_{y,\text{mask}}}{\beta_{y,\text{QC1}}}}\, a_{y,\text{QC1}}, \eta_{y,\text{mask}}\delta_a\right), \tag{32}$$

where $a_{x,\text{QC2}}$ and $a_{y,\text{QC1}}$ are the smallest apertures in the vicinity of the IP in the horizontal and vertical directions, respectively. The movable masks protecting the detector are optimized by the detector background and lifetime in Fig. 9. The detector response is obtained by using the GEANT simulation [20] with the results of particle-tracking simulations in the last procedure.

The contribution from bremsstrahlung scattering due to beam–gas interaction is estimated to be small with respect to that from Coulomb scattering for the detector background. The cross section of Coulomb scattering on nuclei can be expressed by

$$\frac{d\sigma}{d\Omega} = \left(\frac{Zr_e}{2\gamma}\right)^2 \frac{1}{\sin^4\frac{\theta}{2}}, \tag{33}$$

where Z is the atomic number and θ is the scattering angle. If the aperture is asymmetric for the polar angle and has a rectangular shape, the total cross section is written as [21]

$$\sigma(\hat{\theta}_x, \hat{\theta}_y) = 4\left(\frac{Zr_e}{2\gamma}\right)^2 \left(\int_0^{\arctan R} d\phi \int_{\hat{\theta}_x/\cos\phi}^{\pi} \frac{\sin\theta}{\sin^4\frac{\theta}{2}} d\theta + \int_{\arctan R}^{\pi/2} d\phi \int_{\hat{\theta}_y/\sin\phi}^{\pi} \frac{\sin\theta}{\sin^4\frac{\theta}{2}} d\theta\right)$$

$$= \left(\frac{Zr_e}{2\gamma}\right)^2 \frac{8}{\hat{\theta}_y^2} F(R) \tag{34}$$

and

$$F(R) = \pi + (R^2 + 1)\sin(2\arctan R) + 2(R^2 - 1)\arctan R, \tag{35}$$
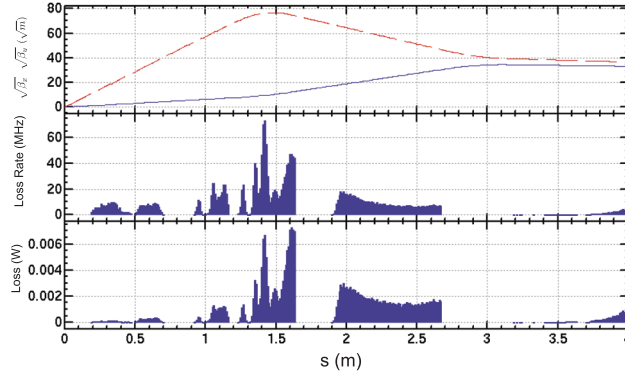
15/17

Fig. 10. Loss rate due to radiative Bhabha events in the vicinity of the IP ($s = 0$) in the HER.

where

$$R = \frac{\hat{\theta}_y}{\hat{\theta}_x} \tag{36}$$

$$\hat{\theta}_x = \frac{a_{x,\mathrm{QC2}}}{\sqrt{\beta_{x,\mathrm{QC2}}\langle\beta_x\rangle}} \tag{37}$$

$$\hat{\theta}_y = \frac{a_{y,\mathrm{QC1}}}{\sqrt{\beta_{y,\mathrm{QC1}}\langle\beta_y\rangle}}. \tag{38}$$

The lifetime can be calculated by

$$\frac{1}{\tau} = c n_g \sigma, \tag{39}$$

where $n_g = 2P/k_B/T$ with $k_B = 1.38 \times 10^{-23}$ (J/K) the Boltzmann constant, P the gas pressure, and T the temperature, a factor of 2 for bi-atomic molecules. The lifetime in the LER, $\tau = 2190$ sec, is obtained with $P = 10^{-7}$ Pa, $T = 300$ K, $Z = 7$, $a_{x,\mathrm{QC2}} = 35$ mm, $a_{y,\mathrm{QC1}} = 13.5$ mm, $\beta_{x,\mathrm{QC2}} = 420$ m, $\beta_{y,\mathrm{QC1}} = 2900$ m, $\langle\beta_x\rangle = 20$ m, and $\langle\beta_y\rangle = 49$ m. The loss rate due to Coulomb scattering with gas molecules is smaller than the Touschek effect in the LER by a factor of 3–4.

The total cross section of a radiative Bhabha process is approximately written as

$$\sigma(\delta_a, \sigma_y^*) = \frac{16\alpha r_e^2}{3} \left\{ \left(\log\frac{1}{\delta_a} - \frac{5}{8}\right)\left(\log\left(\frac{\sqrt{2}m_e\sigma_y^*}{\hbar c}\right) + \frac{\gamma_E}{2}\right) + \frac{1}{4}\left(\frac{13}{3}\log\frac{1}{\delta_a} - \frac{17}{6}\right)\right\}, \tag{40}$$

where α is the fine-structure constant, $\gamma_E = 0.577\cdots$ is Euler's constant, and δ_a is the momentum acceptance of the ring. The above analytic formula includes an impact parameter larger than the vertical beam size. The rate of the radiative Bhabha events is proportional to the luminosity. The luminosity lifetime is 1800 sec, which is obtained from Eq. (40) with $\delta_a = 1.5\%$ and the design parameters in the LER. In order to evaluate the loss rate, both the simulation based on the analytic formula and BBBREM [22], which is a Monte Carlo simulation of radiative Bhabha scattering in the very forward direction, are utilized. Figure 10 shows the beam loss due to radiative Bhabha scattering generated by BBBREM in the HER. The generated particles are tracked using the SAD code.

Synchrotron radiation emitted from the beam in the final-focus system can be the source of detector background. This source is significant in the HER since the beam energy is high and the energy region of the synchrotron radiation is a few keV to tens of keV. The inner surface of the beryllium pipe is coated with a gold plate to absorb the synchrotron radiation before it reaches the inner detectors.

The shape of the IP chamber and the ridge structure are designed to avoid direct synchrotron radiation hits at the beam pipe.

6.   Summary

The concept of the accelerator design for SuperKEKB is presented. The nano-beam scheme is one of the candidates and is a feasible scheme aimed at the target luminosity; it overcomes the hour-glass effect as well as the bunch length related to the coherent synchrotron radiation and the HOM problem. In addition, the five big issues—Touschek lifetime, machine error and optics correction, injection under the influence of beam–beam interaction, detector background, and beam energy—are discussed. SuperKEKB is designed with the nano-beam scheme using the experience gained from KEKB.

References

 [1] KEKB B-Factory Design Report, KEK Report No. 95-7 (1995).
 [2] S. Kurokawa et al., KEK Report No. 2001-157, 2001.
 [3] "SuperB Conceptual Design Report", INFN/AE-07/2, SLAC-R-856, LAL 07-15 (March 2007).
 [4] Y. Suetsugu et al., Nucl. Instrum. Meth. A **578**, 470 (2007).
 [5] M. G. Minty et al., SLAC-PUB-7954 (September 1998).
 [6] D. Brandt et al., CERN SL-99-031 AP (March 1999).
 [7] M. Tawada et al., Conf. Proc. C110904 (2011) 2457 IPAC-2011-WEPO027.
 [8] *Strategic accelerator design*. (Available at: http://acc-physics.kek.jp/SAD.)
 [9] A. Morita et al., Conf. Proc. C110904 (2011) 3691 IPAC-2011-THPZ006.
[10] ANSYS is trademark by CYBERNET Inc. http://www.ansys.com.
[11] H. Yamaoka et al., Conf. Proc. C1205201 (2012) 3548 IPAC-2012-THPPD023.
[12] H. Koiso et al., Conf. Proc. C070625 (2007) 3321 PAC07-THPAN042.
[13] D. Sagan et al., Phys. Rev. ST Accel. Beams **3**, 092801 (2000).
[14] Y. Cai, Phys. Rev. E **68**, 036501 (2003).
[15] Y. Ohnishi et al., Phys. Rev. ST Accel. Beams **12**, 091002 (2009).
[16] H. Sugimoto et al., Conf. Proc. C1205201 (2012) 1203 IPAC-2012-TUPPC020.
[17] S. Mayers, LEP NOTE 334 (November 1981).
[18] P. Collier, CERN-SL-95-50OP (June 1995).
[19] H. Nakayama et al., Conf. Proc. C1205201 (2012) 1825 IPAC-2012-TUPPR007.
[20] S. Agostinelli et al., Nucl. Instrum. Methods Phys. Res., Sect. **506**, 250 (2003).
[21] H. Wiedemann, *Particle Accelerator Physics* (Springer, Berlin, 1993).
[22] R. Kleiss and H. Burkhardt, hep-ph/9401333.